

# Growth and angular dependent resistivity of $\text{Nb}_2\text{Pd}_{0.73}\text{S}_{5.7}$ superconducting state single crystals fiber

Anil K. Yadav<sup>a,b,\*</sup>, Himanshu Sharma<sup>a</sup>, C. V. Tomy<sup>a,†</sup> and Ajay D. Thakur<sup>c</sup>

<sup>a</sup> *Department of physics, Indian Institute of Technology Bombay, Mumbai-400076 India*

<sup>b</sup> *Department of Physics, Ch. Charan Singh University Meerut, Meerut-250004 India and*

<sup>c</sup> *Department of Physics, Indian Institute of Technology Patna, Patna-800013 India*

## Abstract

We report the growth of  $\text{Nb}_2\text{Pd}_{0.73}\text{S}_{5.7}$  superconducting single crystal fibers via slow cooling solid state reaction method. Superconducting transition temperature ( $T_c \sim 6.5\text{K}$ ) is confirmed from magnetization and transport measurements. A comparative study is performed for determination of superconducting anisotropy,  $\Gamma$ , via conventional method (by taking ration of two superconducting parameters) and scaling approach method. Scaling approach, defined within the framework of the Ginzburg-Landau theory is applied to the angular dependent resistivity measurements to estimate the anisotropy. The value of  $\Gamma$  close to  $T_c$  from scaling approach is found to be  $\sim 2.5$  that is slight higher compare to conventional approach ( $\sim 2.2$ ). Further, variation of anisotropy with temperature suggests that it is a type of multi-band superconductor.

---

\*Electronic address: [anilsaciitb@gmail.com](mailto:anilsaciitb@gmail.com)

†Electronic address: [tomy@phy.iitb.ac.in](mailto:tomy@phy.iitb.ac.in)

## I. INTRODUCTION

Ternary chalcogenide of non-superconducting compound  $\text{Nb}_2\text{Pd}_{0.81}\text{Se}_5$  turns into a superconductor with superconducting transition temperature  $T_c \sim 6.5\text{ K}$  when Se is replaced with S [1]. This superconductor has caused a lot of interest to research community due to its extremely large upper critical fields amongst the known Nb based superconductors and shown a possibility to grow long flexible superconducting fibers [1,2]. Structurally, this compound crystallizes in the monoclinic structure with symmetry  $C2/m$  space group [1,2,3]. Its structure comprises laminar sheets, stacked along the b-axis, consisting of Pb, Nb and S atoms. Each sheet contains two unique building blocks of  $\text{NbS}_6$  and  $\text{NbS}_7$  atoms inter-linked by the Pd-atoms [1,3,4]. Yu *et al.*, have constructed the superconducting phase diagram of  $\text{Nb}_2\text{Pd}_{1-x}\text{S}_{5\pm\delta}$  ( $0.6 < x < 1$ ) single crystal fibers by varying composition of Pd and S and found maximum  $T_c \sim 7.43\text{ K}$  in  $\text{Nb}_2\text{Pd}_{1.1}\text{S}_6$  stoichiometry compound [2]. One of the important parameter which needs to be determine precisely for this compound is the anisotropy ( $\Gamma$ ) as it shown extremely large direction dependent upper critical field [1]. In the conventional approach, the anisotropy is determined as ration of two superconducting parameters (such as band dependent effective masses, penetration depth, upper critical fields etc.) in two orientations w.r.t. the crystallographic axes and applied magnetic field [5]. Zhang *et al.*, [1] have determined the temperature dependent anisotropy in this compound using the above conventional method by taking the ratio of  $H_{c2}(T)$  in two orientations. However, in this case, estimation of  $H_{c2}(0)$  is subject to different criteria and formalism which may introduce some uncertainty in the anisotropy ( $\Gamma$ ) calculation [6]. Blatter *et al.*, have given a simple alternate way to estimate the anisotropy of a superconductor, known as the scaling approach [7]. In this approach, any anisotropic data can be changed into isotropic form by using some scaling rule in which only one parameter has to adjust for which all isotropic curves collapse into single curve, that adjusted parameter is anisotropy of superconductor. Thus its limits the uncertainty in the determination of  $\Gamma$  as compared to the conventional approach. Employing scaling approach, Wen et al., have estimated the anisotropy of several Fe-based superconductors such as  $\text{NdFeAsO}_{0.82}\text{F}_{0.18}$  [8],  $\text{Ba}_{1-x}\text{K}_x\text{Fe}_2\text{As}_2$  [6] and  $\text{Rb}_{0.8}\text{Fe}_2\text{Se}_2$  [9]. Shahbazi *et al.*, have also performed similar studies on  $\text{Fe}_{1.04}\text{Se}_{0.6}\text{Te}_{0.4}$  [10] and  $\text{BaFe}_{1.9}\text{Co}_{0.1}\text{As}_2$  [11] single crystals. In this paper, we report the anisotropy estimation of  $\text{Nb}_2\text{Pd}_{0.73}\text{S}_{5.7}$  single crystals via conventional and scaling approach methods near  $T_c$ . We also provide further evidence

that the bulk superconducting anisotropy is not universally constant, but is temperature dependent down to  $T_c$ .

## II. METHOD

Single crystal fibers of  $\text{Nb}_2\text{Pd}_{0.73}\text{S}_{5.7}$  were synthesized via slow cooling of the charge in the solid state reaction method, as reported in reference [1]. Starting raw materials (powder) Nb (99.99%), Pd (99.99%) and S (99.999%) were taken in the stoichiometry ratio of 2:1:6 and mixed in an Ar atmosphere inside a glove box. The well-homogenized powder was sealed in a long evacuated quartz tube and heated to 800°C with a rate of 10°C/h. After the reaction for 24 hours at this temperature, the reactants were cooled down at a rate of 2°C/h to 360°C, followed by cooling to room temperature by switching the furnace off. As-grown samples look like a mesh of small wires when viewed under an optical microscope. Some part of the as-grown sample was dipped in dilute  $\text{HNO}_3$  to remove the bulk material and to pick up a few fiber rods for further measurements. X-ray diffraction (XRD) was performed on powdered  $\text{Nb}_2\text{Pd}_{0.73}\text{S}_{5.7}$  single crystal fibers for structure determination. High energy x-ray diffraction analysis (EDAX) is used to identify the chemical elements and composition. Magnetization measurement was performed using a superconducting quantum interference device - vibrating sample magnetometer (SQUID-VSM, Quantum Design Inc. USA). Angular dependent resistivity was carried out using the resistivity option with horizontal rotator in a physical property measurement system (PPMS) of Quantum Design Inc. USA. Electrical connections were made in four probe configuration using gold wires bonded to the sample with silver epoxy.

## III. RESULTS

### A. Structure analysis

Figure 1(a) shows the scanning electron microscope (SEM) image of  $\text{Nb}_2\text{Pd}_{0.73}\text{S}_{5.7}$  single crystals fibers. It is clear from the image that the fibers are grown in different shapes and lengths. Figure 1(b) shows the XRD patterns of powdered  $\text{Nb}_2\text{Pd}_{0.73}\text{S}_{5.7}$  single crystals. Rietveld refinement was performed on the powder XRD data using  $C2/m$  monoclinic crystal structure of  $\text{Nb}_2\text{Pd}_{0.81}\text{Se}_5$  as reference in the FullProf suite software. The lattice parameters

( $a = 12.154(1)\text{\AA}$ ,  $b = 3.283(7)\text{\AA}$  and  $c = 15.09(9)\text{\AA}$ ) obtained from the refinement are approximately same as reported earlier in reference [1,3], even though the intensities could not be matched perfectly. Peak (200) is found to be the one with the highest intensity even when the XRD was obtained with a bunch of fibers, indicating a preferred crystal plan orientation along the ( $l00$ ) direction in our powdered samples. Similar preferred orientation was also reported for single crystals in reference [2]. This may be the reason for the discrepancy in the intensities between the observed and the fitted XRD peaks. Further, to confirm the single crystalline nature of the fibers, we have taken the selective area electron diffraction (SAED) pattern of the fibers; a typical pattern is shown in Figure 1(c). Nicely ordered spotted diffraction pattern confirms the single crystalline nature of the fibers. Figure 1(d) shows the optical image of a typical cylindrical fiber of diameter  $\sim 1.2\ \mu\text{m}$  and of length  $\sim 1814\ \mu\text{m}$ , which was used for the four probe electrical resistivity measurements (Fig. 1(e) shows the gold wires and silver paste used for the electrical connections). All chemical elements are found to be present in the compound with slight variation from starting composition in EDAX analysis.

## B. Confirmation of superconducting properties

In order to confirm the occurrence of superconductivity in the prepared single crystals, magnetic measurement was performed on a bunch of fibers (as alone single crystal fiber did not give large enough signal in magnetization). Figure 2 shows a part of the temperature dependent zero field-cooled (ZFC) and field-cooled (FC) magnetization measurements at  $H = 200\text{e}$ . The onset superconducting transition temperature ( $T_c^{\text{on};\text{M}}$ ) is observed to be  $\sim 6.5\text{ K}$  which is taken from the bifurcation point of ZFC and FC curves. In order to confirm the superconducting nature of the grown single crystal fibers, resistivity was measured using one of the fibers removed from the ingot. We have plotted a part of resistivity measurement (in zero applied magnetic fields) in Fig. 2 along with the magnetization curve where zero resistivity transition temperature,  $T_c^{\text{zero}}$  matches well with the onset transition temperature of magnetization,  $T_c^{\text{on};\text{M}}$  as well as the  $T_c$  reported in reference [1,2]. However, the onset transition temperature from resistivity ( $T_c^{\text{on}}$  : the temperature at which resistivity drop to 90% from normal state resistivity) is found to be  $\sim 7.8\text{ K}$ , which is comparable to the optimized maximum  $T_c^{\text{on}}$  for this compound reported by Yu *et al.*, [2]. The narrow superconducting

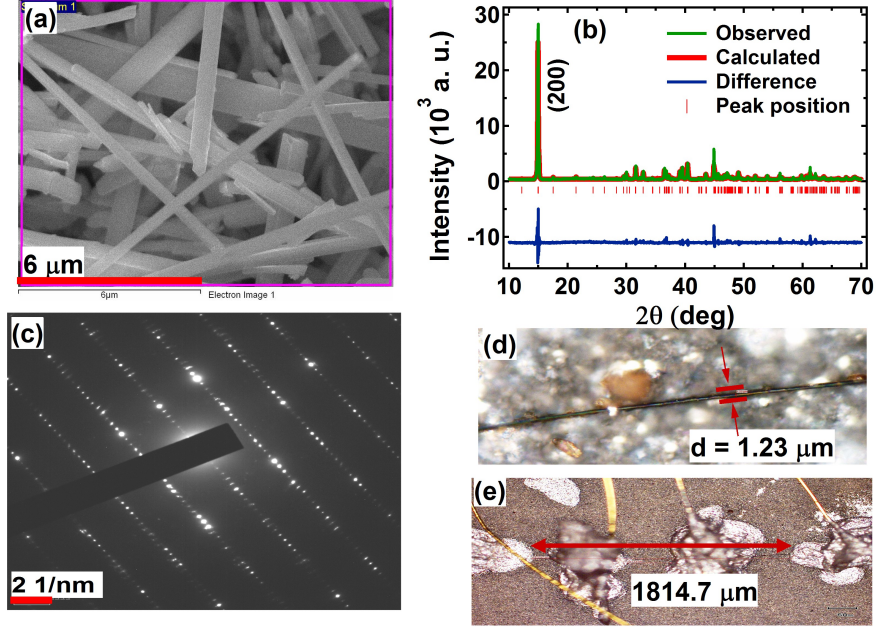


Figure 1: (Color online) (a) SEM image of bunch of single crystal fibers of  $\text{Nb}_2\text{Pd}_{0.73}\text{S}_{5.7}$ . (b) X-ray diffraction patterns: observed (green), calculated (red) and difference (blue) (c) SAED pattern of a single crystal fiber (d) optical image of a typical cylindrical wire used for transport study (e) Four probe connections on a fiber.

transition width ( $\sim 1.3\text{ K}$ ) in resistivity indicates the quality of the single crystal fibers (see Fig. 2). The residual resistivity ratio ( $R_{RR} \approx \frac{R(300\text{ K})}{R(8\text{ K})}$ ), which indicates the metallicity of a material, is found to be  $\sim 3.4$  for our sample. This value of RRR is much less than the corresponding value for good conductors, that categorized it as bad metals.

### C. Angular dependent transport properties

In order to estimate the superconducting anisotropy properties, we have to assign single crystal fibers orientation axis. Since we cannot assign a growth direction for our cylindrical single crystal fibers from XRD due to very fine single crystals therefore we have adopted b-axis along length of fibers as given in reference [1] because of same synthesis method is followed to grow these single crystal fibers. Figures 3(a) and 3(c) show the resistivity plots as function of temperature in different applied magnetic fields from zero to 90 kOe along  $H \parallel$  b-axis and  $H \perp$  b-axis. Three transition temperatures,  $T_c^{\text{on}}$ ,  $T_c^{\text{mid}}$  and  $T_c^{\text{off}}$  are marked in the figure using the criteria,  $90\%\rho_n$ ,  $50\%\rho_n$  and  $10\%\rho_n$  (where  $\rho_n$  is normal state resistivity

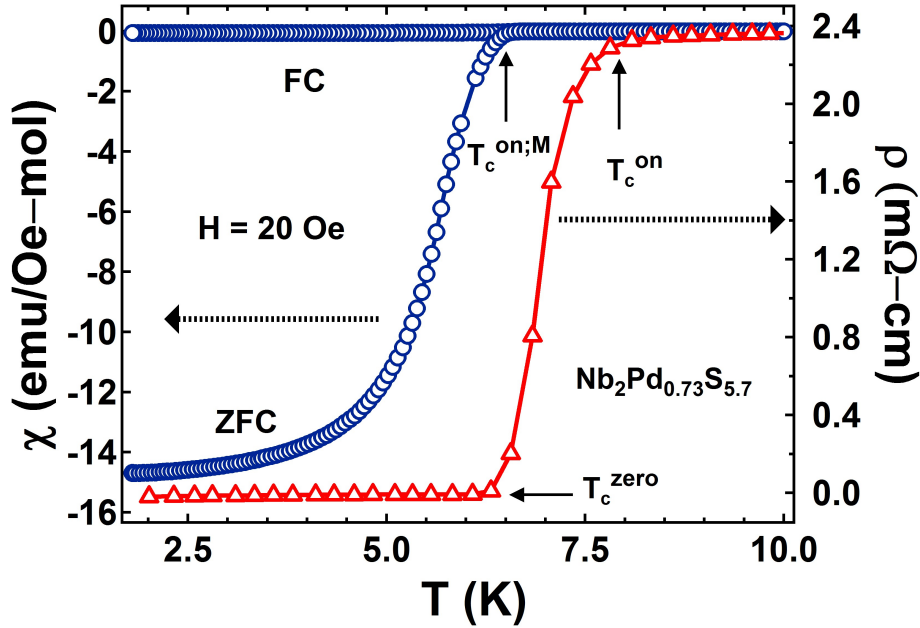


Figure 2: (Color online) Zero field-cooled (ZFC) and field-cooled (FC) magnetization curves at 20 Oe (open circle) and resistivity measurement at zero field (open triangle). Onset superconducting transition temperature,  $T_c^{\text{on};M}$ , from magnetization and zero resistivity transition temperature,  $T_c^{\text{zero}}$ , from resistivity measurements confirm the  $T_c$  of  $\text{Nb}_2\text{Pd}_{0.73}\text{S}_{5.7}$  superconductor.

at 8 K), respectively. The  $T_c$  shifts toward the lower temperatures as field increases with the rate of 0.05 K/kOe and 0.02 K/kOe along  $H \parallel b$ -axis and  $H \perp b$ -axis, respectively. The  $H$ - $T$  phase diagrams are plotted at three transition temperatures in Figs. 3(b) and 3(d) for both the orientations. In order to find out upper critical fields ( $H_{c2}(0)$ ), these  $H$ - $T$  curves are fitted with the empirical formula,  $H_{c2}(0) = H_{c2}(T)(1 - (T/T_c)^2)$  [1, 2], further these fitted curves have been extrapolated to the zero temperature to extract the  $H_{c2}(0)$  values, that come out to be  $\sim 180$  kOe and  $\sim 390$  kOe at  $T_c^{\text{on}}$  along  $H \parallel b$ -axis and  $H \perp b$ -axis, respectively. Conventionally the anisotropy is found to be  $\sim 2.2$ , estimated by taking ratio of  $H_{c2}(0)$  values in two orientations. In order to corroborate the  $\Gamma$  values further, we have measured the angular dependent resistivity  $\rho(\theta)$  at different magnetic fields at certain temperatures close to  $T_c$ .

The insets of Figs. 4(a), (b), (c) and (d) show  $\rho(\theta)$  curves at 10 kOe, 30 kOe, 50 kOe, 70 kOe and 90 kOe for  $T = 5.0$  K, 5.5 K, 6.0 K and 6.5 K, respectively. All the  $\rho(\theta)$  curves show a symmetric dip at  $\theta = 90^\circ$  and a maximum at  $0^\circ$  and  $180^\circ$ . In all the curves, the center

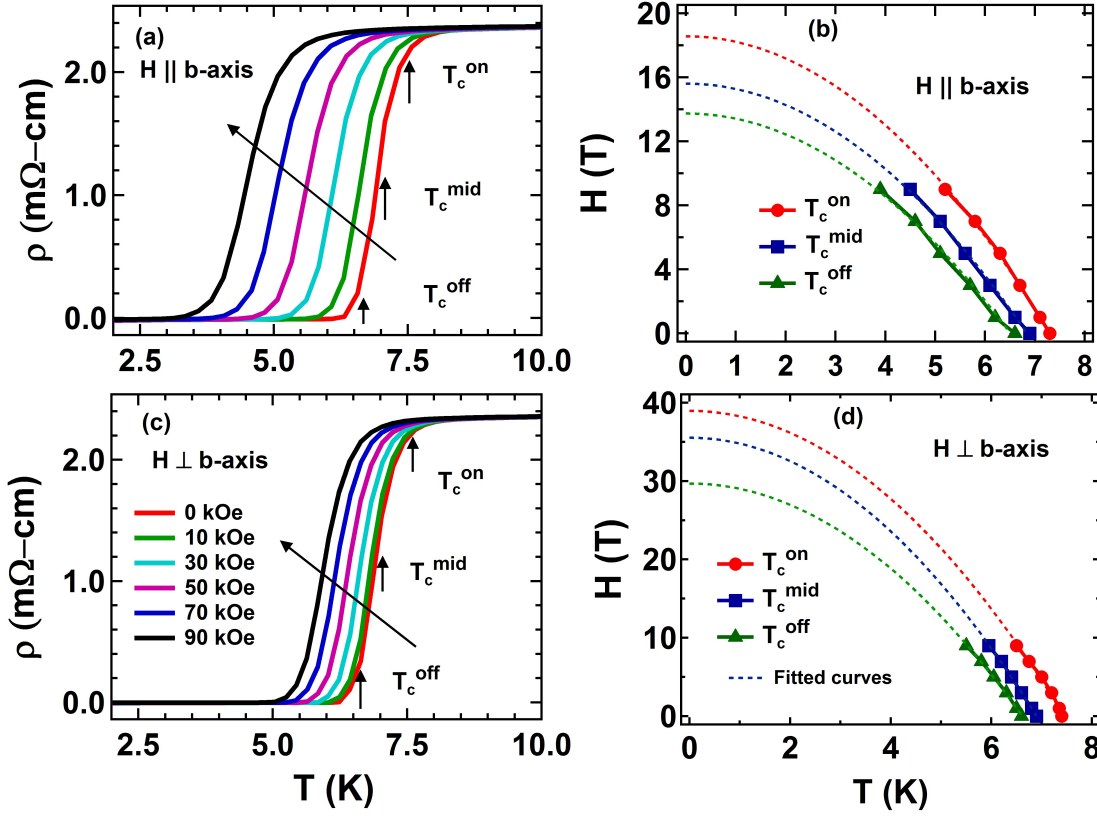


Figure 3: (Color online) Temperature dependent resistivity plots at different applied fields vary from 0 kOe to 90 kOe (a) for  $H \parallel b$ -axis (c) for  $H \perp b$ -axis. (b) and (d) plots show  $H$ - $T$  phase diagrams at  $T_c^{\text{on}}$ ,  $T_c^{\text{mid}}$  and  $T_c^{\text{off}}$  transition temperatures. Dashed curves show the fitting curves corresponding empirical formula,  $H_{c2}(0) = H_{c2}(T)(1 - (T/T_c)^2)$ .

of the dip shifts from zero to non-zero resistivity as the temperature and field increases. The main panel of the Fig. 4 shows rescaled  $\rho(\theta)$  curves of 10 kOe, 30 kOe, 50 kOe, 70 kOe and 90 kOe fields at temperatures (a) 5.0 K (b) 5.5 K (c) 6.0 K and (d) 6.5 K, respectively using the rescaling function:

$$\tilde{H} = H \sqrt{\sin^2\theta + \Gamma^2\cos^2\theta} \quad (1)$$

where  $\Gamma$  is anisotropy and  $\theta$  is angle between the field and crystal axis. All rescaled curves at fixed temperature are now isotropic, i.e., all curves collapse on the single curve. In this method only anisotropic parameter,  $\Gamma$ , was adjusted to convert data into the isotropic form, that value of  $\Gamma$  is the anisotropy at that temperature. Figure 5 shows temperature dependent anisotropy ( $\Gamma(T)$ ) plot which is obtained from the angular resistivity data. Anisotropy decreases slowly as the temperature goes down in superconducting state. As Zhang *et al.* [1]



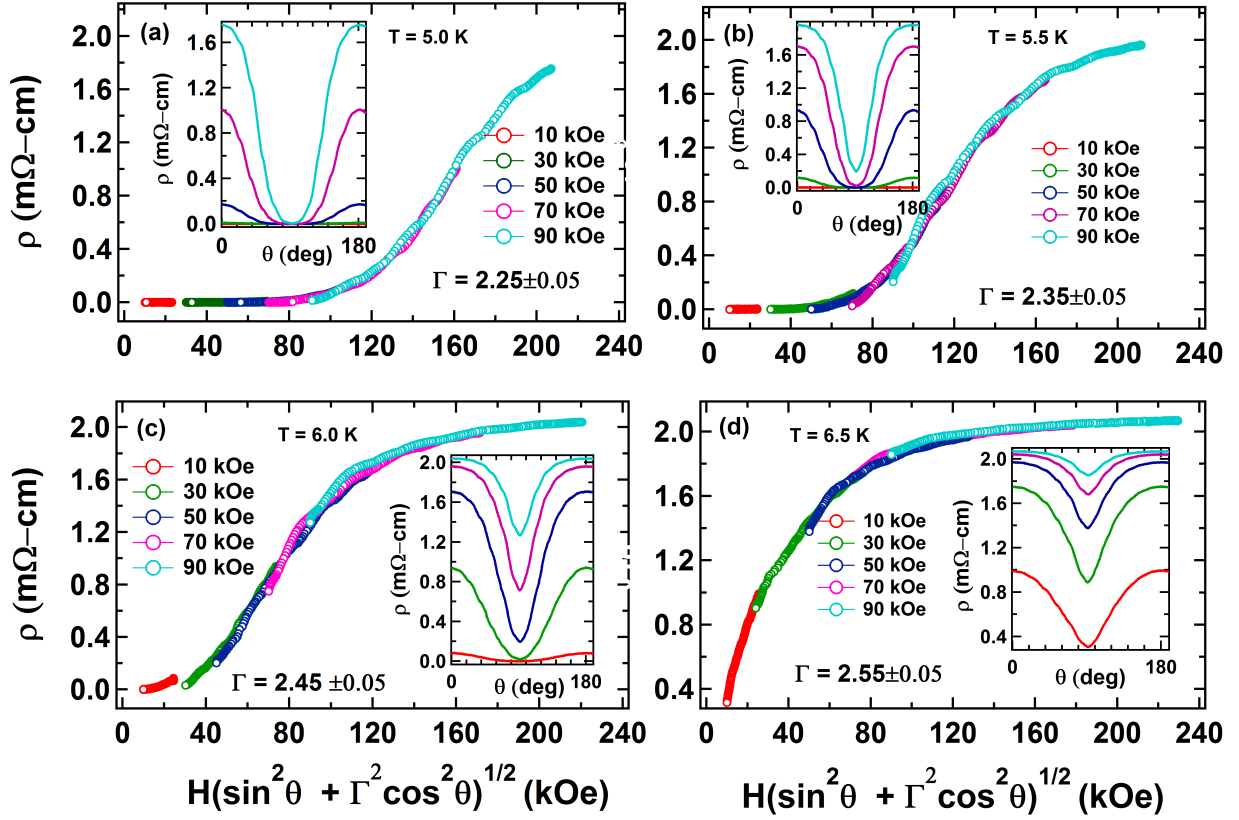


Figure 4: (Color online) Insets of figure (a) to (d) show resistivity ( $\rho$ ) plots as a function of angle,  $\theta$  (angle between b-axis and applied magnetic fields) at fields 10 kOe, 30 kOe, 50 kOe, 70 kOe and 90 kOe for temperatures (a) 5 K (b) 5.5 K (c) 6.0 K and (d) 6.5 K and main panels of figure show the resistivity plots as function of scaling field  $\tilde{H} = H \sqrt{\sin^2\theta + \Gamma^2\cos^2\theta}$ .

have explained that this dependency of anisotropy in temperature may be due to the opening of superconducting gap of different magnitude on different Fermi surface sheets where each associated with bands of distinct electronic anisotropy. Li *et al.*, have reported similar temperature dependent anisotropy behavior for  $\text{Rb}_{0.76}\text{Fe}_2\text{Se}_{1.6}$ ,  $\text{Rb}_{0.8}\text{Fe}_{1.6}\text{Se}_2$ ,  $\text{Ba}_{0.6}\text{K}_{0.4}\text{Fe}_2\text{As}_2$ ,  $\text{Ba}(\text{Fe}_{0.92}\text{Co}_{0.08})_2\text{As}_2$  single crystals and explained that this may be due to the multiband effect or gradual setting of pair breaking due to spin-paramagnetic effect [9]. Shahbazi *et al.*, have also reported similar results for  $\text{Fe}_{1.04}\text{Te}_{0.6}\text{Se}_{0.4}$  and  $\text{BaFe}_{1.9}\text{Co}_{0.8}\text{As}_2$  single crystal through angular dependent transport measurements [10,11]. Various theoretical models for study of Fermi surface have supported the presence of multiband superconducting gap in Fe-based superconductors [12,13,14]. Here, the density functional theory (DFT) calculation indeed has shown that the  $\text{Nb}_2\text{Pd}_{0.81}\text{S}_5$  superconductor is a multi-band superconductor [1].



Compared to  $\text{MgB}_2$  [15,16] and cuprate superconductors [17] the anisotropy of  $\text{Nb}_2\text{Pd}_{0.73}\text{S}_{5.7}$  is very small; however, it is comparable with some of the iron based (Fe-122 type) superconductors [9].

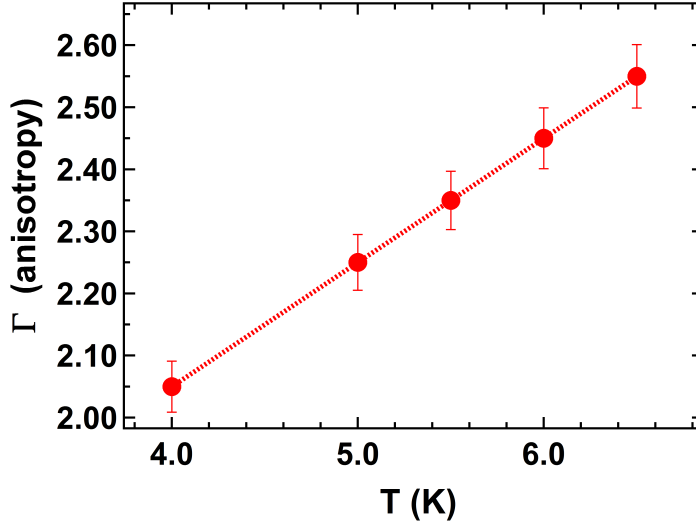


Figure 5: (Color online) Anisotropy variation with temperature measured from angular dependent resistivity.

#### IV. CONCLUSIONS

In conclusion, we have successfully synthesized the  $\text{Nb}_2\text{Pd}_{0.73}\text{S}_{5.7}$  single crystal fibers via slow cooling solid state reaction method. Superconducting properties of sample have been confirmed via magnetic and transport measurements. Conventionally, upper critical fields are measured from magneto-transport study. Angular dependence of resistivity are measured in presence of magnetic fields at different temperatures in superconducting state which further rescaled using a scaling function to convert isotropic form that direct provides anisotropy. The anisotropy is found to be  $\sim 2.5$  near  $T_c$  which is less  $\sim 2.2$  compare to achieve from conventional method. Anisotropy decreases slowly with decreasing temperature, which is attributed to the multi-band nature of the superconductor.

## Acknowledgments

AKY would like to thank CSIR, India for SRF grant.

---

- [1] Q. Zhang, G. Li, D. Rhodes, A. Kiswandhi, T. Besara, B. Zeng, J. Sun, T. Siegrist, M. D. Johannes, L. Balicas, *Scientific Reports*, **3**, 1446 (2013). H. Yu, M. Zuo, L. Zhang, S. Tan, C. Zhang, Y. Zhang, *J. Am. Chem. Soc.* **135**, 12987 (2013).
- [2] H. Yu, M. Zuo, L. Zhang, S. Tan, C. Zhang, Y. Zhang, *J. Am. Chem. Soc.* **135**, 12987 (2013).
- [3] R. Jha, B. Tiwari, P. Rani, V. P. S. Awana, arXiv:1312.0425 (2013).
- [4] D. A. Keszler, J. A. Ibers, M. Y. Shang and J. X. Lu, *J. solid state chem.* **57**, 68 (1985).
- [5] W. E. Lawrence and S. Doniach, in *Proceedings of the 12th International Conference Low Temperature Physics*, edited by E. Kanda Keigaku, Tokyo (1971).
- [6] Z. S. Wang, H. Q. Luo, C. Ren, H. H. Wen, *Phys. Rev. B* **78**, 140501(R) (2008).
- [7] G. Blatter, V. B. Geshkenbein, and A. I. Larkin, *Phys. Rev. Lett.* **68**, 875 (1992).
- [8] Y. Jia, P. Cheng, L. Fang, H. Yang, C. Ren, L. Shan, C. Z. Gu, H. H. Wen, *Sup. Science and Technology* **21**, 105018 (2008).
- [9] C. H. Li, B. Shen, F. Han, X. Zhu, and H. H. Wen, *Phys. Rev. B* **83**, 184521 (2011).
- [10] M. Shahbazi, X. L. Wang, S. X. Dou, H. Fang, and C. T. Lin, *J. Appl. Phys.* **113**, 17E115 (2013).
- [11] M. Shahbazi, X. L. Wang, S. R. Ghorbani, S. X. Dou, and K. Y. Choi, *Appl. Phys. Lett.* **100**, 102601 (2012).
- [12] Q. Han, Y. Chen and Z. D. Wang, *EPL* **82**, 37007 (2008).
- [13] C. Ren, Z. S. Wang, H. Q. Luo, H. Yang, L. Shan, and H. H. Wen, *Phys. Rev. Lett.* **101**, 257006 (2008).
- [14] V. Cvetkovic, Z. Tesanovic, *Europhysics Letters* **85**, 37002 (2009).
- [15] A. Rydh, U. Welp, A. E. Koshelev, W. K. Kwok, G. W. Crabtree, R. Brusetti, L. Lyard, T. Klein, C. Marcenat, B. Kang, K. H. Kim, K. H. P. Kim, H.-S. Lee, and S.-I. Lee, *Phys. Rev. B* **70**, 132503 (2004).
- [16] K. Takahashi, T. Atsumi, N. Yamamoto, M. Xu, H. Kitazawa, and T. Ishida, *Phys. Rev. B* **66**, 012501 (2002).

[17] C. P. Poole, Jr. H. A. Farach, J. Richard. Creswick, Superconductivity (Elsevier) (2007).